2015

Multi-scale evaluation of light use efficiency in MODIS gross primary productivity for croplands in the Midwestern United States

Qinchuan Xin
Tsinghua University, Beijing, xqcchina@gmail.com

Mark Broich
University of New South Wales, Sydney, mark.broich@unsw.edu.au

Andrew E. Suyker
University of Nebraska-Lincoln, asuyker1@unl.edu

Le Yu
Tsinghua University, Beijing

Peng Gong
University of California, Berkeley, penggong@berkeley.edu

Follow this and additional works at: http://digitalcommons.unl.edu/natrespapers

Part of the Climate Commons, Environmental Monitoring Commons, Other Environmental Sciences Commons, and the Other Oceanography and Atmospheric Sciences and Meteorology Commons

Multi-scale evaluation of light use efficiency in MODIS gross primary productivity for croplands in the Midwestern United States

Qinchuan Xin,[1] Mark Broich,[2] Andrew E. Suyker,[3] Le Yu,[1] and Peng Gong[1,4]

1 Center for Earth System Science, Tsinghua University, Beijing, China
2 University of New South Wales, Sydney, Australia
3 School of Natural Resources, University of Nebraska–Lincoln, Lincoln, NE, USA
4 Environmental Science, Policy and Management and Geography, University of California, Berkeley, CA, USA

Corresponding authors — Q. Xin & P. Gong, Tsinghua University, Mengminwei South Building, Room 920, Beijing 100084, China; tel +86 1 881 025 3088, email xqcchina@gmail.com (Q. Xin) penggong@berkeley.edu (P. Gong).

Abstract

Satellite remote sensing provides continuous observations of land surfaces, thereby offering opportunities for large-scale monitoring of terrestrial productivity. Production Efficiency Models (PEMs) have been widely used in satellite-based studies to simulate carbon exchanges between the atmosphere and ecosystems. However, model parameterization of the maximum light use efficiency (ε^*_{GPP}) varies considerably for croplands in agricultural studies at different scales. In this study, we evaluate cropland ε^*_{GPP} in the MODIS Gross Primary Productivity (GPP) model (MOD17) using in situ measurements and inventory datasets across the Midwestern US. The site-scale calibration using 28 site-years tower measurements derives ε^*_{GPP} values of 2.78 ± 0.48 gC MJ^{-1}($\pm$ standard deviation) for corn and 1.64 ± 0.23 gC MJ^{-1}for soybean. The calibrated models could account for approximately 60–80% of the variances of tower-based GPP. The regional-scale study using 4-year agricultural inventory data suggests comparable ε^*_{GPP} values of 2.48 ± 0.65 gC MJ^{-1} for corn and 1.18 ± 0.29 gC MJ^{-1} for soybean. Annual GPP derived from inventory data (1848.4 ± 298.1 gC m^{-2}y^{-1} for corn and 908.9 ± 166.3 gC m^{-2}y^{-1} for soybean) are consistent with modeled GPP (1887.8 ± 229.8 gC m^{-2}y^{-1} for corn and 849.1 ± 122.2 gC m^{-2}y^{-1} for soybean). Our results are in line with recent studies and imply that cropland GPP is largely underestimated in the MODIS GPP products for the Midwestern US. Our findings indicate that model parameters (primarily ε^*_{GPP}) should be carefully recalibrated for regional studies and field-derived ε^*_{GPP} can be consistently applied to large-scale modeling as we did here for the Midwestern US.

Keywords: Remote sensing, Net primary production, Crop yield, Flux tower, National inventory

1. Introduction

Characterization of the spatial and temporal patterns in terrestrial gross primary production (GPP) and net primary production (NPP) is essential to understand and quantify the carbon exchange between the atmosphere and terrestrial ecosystems (Beer et al., 2010; Lobell et al., 2002). Satellite remote sensing provides spatially continuous and temporally repetitive observations of land surfaces, and has become increasingly important for monitoring vegetation photosynthetic activities over large geographic regions. In satellite-based studies, Production Efficiency Models (PEMs) have been widely employed to estimate terrestrial productivity (Field et al., 1995; Goetz et al., 1999; Gower et al., 2001; Potter et al.,1993; Prince and Goward, 1995; Running et al., 2000, 2004).

The underlying theory behind a variety of PEMs is that vegetation GPP/NPP is linearly related to the amount of photosynthetically active radiation (PAR) absorbed by the canopy:

$$GPP = \varepsilon^*_{GPP} \times f(\varepsilon) \times PAR \times FPAR \qquad (1)$$

where the ε^*_{GPP} (gC MJ^{-1}) value for the GPP calculation is the maximum light use efficiency (LUE) when the environment is not limiting for plant carbon uptake; PAR (MJ) is the photosynthetically active radiation incident on the canopy; FPAR (dimensionless) is the fraction of incident PAR absorbed by the canopy; and $f(\varepsilon)$ (dimensionless) is a scalar that accounts for the effects of environmentalstress and is formulated differently in various PEMs.

However, parameterization of ε^*_{GPP}, a key component in these models, differs widely for croplands in studies at different scales. Typical ε^*_{GPP} in site-scale studies range from 2.40 to 4.24 gC MJ^{-1} for C4 crops and 1.41 to 1.96 gC MJ^{-1} for C3 crops (Chen et al., 2011; Kalfas et al.,

2011; Lindquist et al., 2005; Singer et al.,2011; Turner et al., 2002), while ε^*_{GPP} in many large-scale modeling efforts are about 0.604–1.08 gC MJ^{-1} for croplands (Bradford et al., 2005; Heinsch et al., 2003; Lobell et al., 2002; Zhao and Running, 2010). Note that the ε^*_{GPP} values prescribed in many large-scale biogeochemical models are only approximately half of those in a number of small-scale studies. The discrepancy regarding the ε^*_{GPP} values at different scales may result in biased GPP estimates for croplands. In a recent study, GPP estimates derived from sun-induced chlorophyll fluorescence datasets were approximately 50–75% higher than results from state-of-the-art carbon cycle models, like the MODIS (Moderate Resolution Imaging Spectroradiometer) GPP/NPP product (Guanter et al., 2014). Bandaruet al. (2013) found that modeled NPP in Illinois and Iowa were 2.4 and 1.1 times greater than the MODIS GPP/NPP product for corn and soybean, respectively. However, model evaluation did not identify significant biases in other biomes (Sjöström et al., 2013; Turner et al., 2006), which implies that the differences between field and satellite LUE estimates are the most pronounced in croplands (Garbulsky et al., 2010).

Given the importance of the LUE in modeling cropland productivity, there is a need to investigate reasons for the inconsistent ε^*_{GPP} values in studies at different scales. Most validation efforts for MODIS GPP have been made using eddy covariance data from flux tower measurements, and some studies suggest increasing the ε^*_{GPP} values in models to estimate cropland GPP (Chen et al., 2011; Zhang et al., 2008). On the other hand, some large-scale modeling studies identified overestimations of crop productivity in comparison with statistical inventory data when applying field-derived ε^*_{GPP} values (Lobell et al., 2002; Ruimy et al., 1994; Turner et al., 2006). However, two recent studies that incorporate fine-resolution land use maps and coarse-resolution MODIS data recommend applying field-estimated LUE values for large-scale cropland modeling (Bandaru et al., 2013; Xin et al., 2013).

The objective of this paper is to evaluate cropland ε^*_{GPP} in the MOD17 model at different scales. We perform model calibrations across the Midwestern US using both independent in situ measurements and regional statistical datasets. This would help generate multiple lines of evidence to determine appropriate ε^*_{GPP} values for cropland GPP estimates.

2. Materials and methods

2.1. The MODIS GPP (MOD17) model

Among a variety of PEMs (Cramer et al., 1999; Wu et al., 2010; Yang et al., 2013), we employed the MOD17 model (Running et al., 2004) developed by the Numerical Terradynamic Simulation Group (NTSG) at the University of Montana (UMT). The MOD17 model is used to provide GPP/NPP estimates from MODIS data at 8-day and yearly time steps. In addition to Eq. (1), this model uses the following equations to down-regulate the influences of environmental factors on light use efficiency:

$$f(\varepsilon) = TMIN_s \times VPD_s \qquad (2)$$

where $TMIN_s$ and VPD_s are the attenuation scalars for the daily minimum temperature ($TMIN$) and daily vapor pressure deficit (VPD). These values are calculated with the following simple linear ramp functions:

$$TMIN_s = \frac{TMIN - TMIN_{min}}{TMIN_{max} - TMIN_{min}} \qquad (3)$$

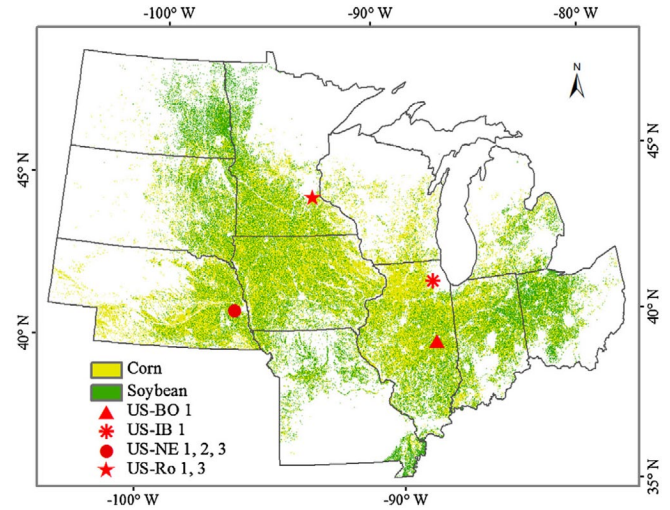$$VPD_s = \frac{VPD_{max} - VPD}{VPD_{max} - VPD_{min}} \qquad (4)$$

Figure 1. Study site locations in the Midwestern US. The corn and soybean maps are shown for 2011 and are derived from the NASS Cropland Data Layer datasets. Site codes are specified in Table 1.

where $TMIN_{max}$ and $TMIN_{min}$ are daily minimum temperatures at $\varepsilon_{GPP} = \varepsilon^*_{GPP}$ and $\varepsilon_{GPP} = 0$, respectively; and VPD_{max} and VPD_{min} are daylight vapor pressure deficits at $\varepsilon_{GPP} = 0$ and $\varepsilon_{GPP} = \varepsilon^*_{GPP}$, respectively.

The MOD17 model prescribes specific parameters in a Biome-Properties-Look-Up-Table (BPLUT) for each biome category. For cropland in MOD17 Collection 5.1, the ε^*_{GPP}, $TMIN_{min}$, $TMIN_{max}$, VPD_{min}, and VPD_{max} are defaulted as 1.044 gC MJ^{-1}, −8.00°C, 12.02°C, 650 Pa, and 4300 Pa, respectively (Zhao and Running, 2010). FPAR data are derived from the upstream MOD15 products (Myneni et al., 2002). Meteorological data such as air temperature, VPD, and incident shortwave radiation come from National Center for Environmental Prediction – Department of Energy (NCEP-DOE) Reanalysis II datasets — http://www.esrl.noaa.gov/psd/data/gridded/data.ncep.reanalysis2.html

2.2. Flux tower site data

We analyzed seven agricultural sites in the Midwestern US (Figure 1; Table 1) that had Level 4 products available in the AmeriFlux database — http://ameriflux.ornl.gov/ . These flux tower sites are operated under different management practices (crop rotations and rainfed/irrigation) and are representative of the widespread agricultural environment in the study area. The AmeriFlux Level 4 products consist of gap-filled meteorological variables and GPP estimates. Missing data due to unsuitable micrometeorological conditions or equipment failures are gap-filled using the marginal distribution sampling method (Reichstein et al., 2005). Flux tower GPP estimates are calculated as the difference between the measured net ecosystem exchange and the estimated ecosystem respiration. Required meteorological variables in the MOD17 model were processed from the half-hour to 8-day datasets to be consistent with the MODIS data.

According to previous studies (Bandaru et al., 2013; Chenet al., 2011), we extracted time series of satellite-derived parameters from Terra/MODIS products for the pixels containing the tower sites. The used Terra/MODIS products included the 8-day 500 m surface reflectance product (MOD09A1), the 8-day 1000 m FPAR/LAI product (MOD15A2), and the 8-day 1000 m vegetation productivity product (MOD17A2). Observations during cloudy conditions within the study period are identified by quality assurance data and gap-filled using lin-

Table 1. Information for the studied tower sites.

Site ID	Site name	Lat (°N)	Lon (°W)	Crops	Irrigation	Period	References
US-Bo1	Bondville	40.0062	88.2904	Corn, soybean		01–06	Meyers and Hollinger (2004)
US-IB1	Fermi Agricultural	41.8593	88.2227	Corn, soybean		06–07	Matamala et al. (2008)
US-Ne1	Mead Irrigated	41.1650	96.4766	Corn	Yes	01–05	Suyker and Verma (2012)
US-Ne2	Mead Irrigated Rotation	41.1649	96.4701	Corn, soybean	Yes	01–05	Suyker and Verma (2012)
US-Ne3	Mead Rainfed	41.1797	96.4396	Corn, soybean		01–05	Suyker and Verma (2012)
US-Ro1	Rosemount G21	44.7143	93.0898	Corn, soybean		04–06	Griffis et al. (2004)
US-Ro3	Rosemount G19	44.7217	93.0893	Corn		05	Griffis et al. (2004)

ear functions (Kalfas et al., 2011). GPP estimates in MOD17A2 are 8-day sums of daily values for each pixel and are divided by a scale factor of 8 to obtain the daily averages. Details regarding these products can be found on the MODIS data website (https://lpdaac.usgs.gov/products/modis products table/).

2.3. Regional data

Agricultural inventory data provide alternative references for crop production throughout the growing season. The 4-year (2009–2012) statistical data for corn and soybean production were obtained for each county from the NASS Quick Stats database — http://www.nass.usda.gov/Quick Stats/ . The NASS datasets have been used widely for regional crop GPP/NPP modeling (Bandaru et al., 2013; Lobell et al., 2002). To exclude regions with sparse agriculture, our analysis was confined to counties with at least 10% of the total area planted in corn and soybean (661 counties were analyzed). Following methods outlined in previous agricultural studies (Prince et al., 2001; Reeves et al., 2005), we translated the reported grain productions to annual GPP. The translation takes equations that are analogous to the allometric equations for forest biomass estimation as follows:

$$\text{GPP} = \left(\frac{Y}{\text{HI}} + \frac{Y}{\text{HI}} \times \text{RS}\right) \times (1 - \text{MC}) \times \frac{\text{CCB}}{\text{CUE}} \quad (5)$$

where Y is the reported crop yields; MC is the moisture content of the grain; RS is the root to shoot ratio; HI is the harvest index; CUE (carbon use efficiency) is the ratio of NPP to GPP; and CCB (carbon content in biomass) is the percentage of dry biomass composed of carbon. In our translation, the carbon content in biomass is estimated as 45% (Schlesinger and Bernhardt, 2013). The ratio of NPP to GPP is estimated as 46% for all crops (Bandaru et al., 2013; Choudhury, 2000). Values for the other parameters were obtained from Lobell et al. (2002).

Crop-specific land use maps have shown potential for improving satellite estimates of crop yields (Bandaru et al., 2013; Xinet al., 2013). Different from the MODIS GPP products that use global land cover maps at 1 km resolution, we use fine-resolution land-use maps from the NASS Cropland Data Layer (CDL) program for regional modeling. The NASS CDL produces crop-specific land use maps for each calendar year at a spatial resolution of 30 or 56 m for the United States based on the classification of multi-sensor satellite imagery with training data from extensive ground surveys. The reported producer's and user's accuracies are 97.1% and 98.6% for corn, and 96.4% and 97.4% for soybean, respectively (Boryan et al.,2011). Fine-resolution CDL maps are mosaicked, re-projected, and scaled up to coarser resolution as percentage maps in the MODIS sinusoidal projection.

2.4. Model setup

Our primary goal in this study is to evaluate $\varepsilon^*_{\text{GPP}}$ for modeling cropland GPP at different scales. GPP references are derived from both flux tower measurements and statistical inventory data. We fit linear regressions with no intercept between GPP and the product of PAR × FPAR

$\times f(\varepsilon)$ to derive the optimal $\varepsilon^*_{\text{GPP}}$ value by minimizing the squared errors (Sjöström et al., 2013). GPP estimates from there calibrated models are further compared with the reference data. To examine factors that influence the $\varepsilon^*_{\text{GPP}}$ and GPP estimates, we set up different inputs for the MOD17 model at both site and regional scales (Table 2). These model setups are further explained in the following sections.

2.4.1. Site modeling

Evaluation efforts have identified several factors that may contribute to the differences between GPP derived from MODIS and flux tower data. Important factors include the model structures (Running et al., 2004), errors in the upstream input data (Sjöströmet al., 2013; Zhao et al., 2005), MODIS sensor viewing angles (Zhanget al., 2014), and the mismatches between the footprints of tower sites and MODIS pixels (Gelybó et al., 2013).

To quantify these effects, we gradually replaced the satellite-derived and meteorological inputs in the MOD17 model and compared modeled GPP estimates with flux tower measurements (Table 2). First, we calibrate the MOD17 model by performing a reference run with inputs the same as MOD17A2 (NCEP-MOD15). Second, because the MOD17 model relies on MOD15 FPAR inputs,we employ the method of Vegetation Photosynthesis Model (Xiaoet al., 2004) to model FPAR as a linear function of Enhanced Vegetation Index (EVI; Eq. (6)). EVI has been found to perform better than NDVI in terms of explaining the seasonal dynamics of carbon exchange in croplands (Bandaru et al., 2013; Kalfas et al., 2011), because EVI minimizes the influences of residual atmospheric contamination and accounts for the variability in soil background reflectance (Huete et al., 2002). EVI at 1 km was calculated based on the mean MOD09A1 band reflectance of four pixels at 500 m. Third, because of the effects of spatial variability, the mismatch in the footprints between the flux tower and MODIS could influence model validation. We performed analysis at 500 m resolution instead of 1000 m resolution because examination of the land use maps indicates that the extent of crop fields is relatively homogeneous at 500 m resolution. Finally, to understand the influence of meteorological inputs (incoming solar radiation, minimum temperature and vapor pressure deficit) on GPP modeling, we use the daily meteorological data from the Ameriflux Level 4 products rather than the NCEP-DOE Reanalysis II dataset, where incident PAR is estimated as 45% of measured incoming shortwave solar radiation (Heinschet al., 2003). Overall, we used six MOD17 model setups for GPP and $\varepsilon^*_{\text{GPP}}$ estimates.

The following linear function of the EVI is used as an alternative method in the Vegetation Photosynthesis Model for estimating FPAR during the photosynthetic active period:

$$\text{FPAR} = a \times \text{EVI} \quad (6)$$

where a is the coefficient constant and is assumed to be 1.0 (Xiaoet al., 2004).

2.4.2. Regional modeling

Regional studies have found that the MODIS GPP estimates are constrained by upstream datasets such as the MODIS FPAR product and

Table 2. Overview of model setups. The used meteorology data include downward shortwave solar radiation, temperature, and vapor pressure deficit.

Model codes	GPP reference	Meteorology data	FPAR	Land cover maps	Resolution
NCEP-MOD15	Eddy covariance	NCEP-DOE reanalysis II	MOD15		1000 m
NCEP-EVI1000	Eddy covariance	NCEP-DOE reanalysis II	EVI		1000 m
NCEP-EVI500	Eddy covariance	NCEP-DOE reanalysis II	EVI		500 m
Local-MOD15	Eddy covariance	Local measurements	MOD15		1000 m
Local-EVI1000	Eddy covariance	Local measurements	EVI		1000 m
Local-EVI500	Eddy covariance	Local measurements	EVI		500 m
MOD15-Mask	National inventory	NCEP-DOE reanalysis II	MOD15	Binary mask	1000 m
EVI-Mask	National inventory	NCEP-DOE reanalysis II	EVI	Binary mask	1000 m
MOD15-Frac	National inventory	NCEP-DOE reanalysis II	MOD15	Fractional cover	1000 m
EVI-Frac	National inventory	NCEP-DOE reanalysis II	EVI	Fractional cover	1000 m

the MODIS land cover product (Zhao et al., 2005). To evaluate these effects, we conducted four model runs across the Midwestern US (Table 2; Figure 1). A reference run (MOD15-Mask) is performed using the same meteorological and satellite-derived inputs as the MODIS GPP product by applying a general cropland mask. The general cropland mask is defined for pixels with more than 50% fractional cover of corn or soybean. For the purpose of comparison, we also run the model with EVI-based FPAR to understand how satellite-derived FPAR may influence ε^*_{GPP} and annual GPP estimates.

In the above two experiments, applying general cropland masks may not account for the effects of pixel variability because crop species under different photosynthetic pathways (C3 and C4) may have varied GPP, and because the typical crop fields are smaller than the 1 km spatial resolution of the MODIS products. To investigate the influences of land-cover/land-use maps, we also derive ε^*_{GPP} and GPP estimates by applying fractional cropland maps derived from NASS CDL datasets. The use of the relatively new NASS CDL dataset allows us separate GPP contributions from corn and soybean for each pixel. Here we implement the hybrid method proposed by Turner et al. (2002) and model GPP as an area-weighted value based on fractional land use maps:

$$\text{GPP} = \sum f_i \times \varepsilon^*_{GPP i} \times f(\varepsilon) \times \text{PAR} \times \text{FPAR} \qquad (7)$$

where $\varepsilon^*_{GPP i}$ is the maximum light use efficiency for crop species i, and f_i is the fractional cover for crop species i.

3. Results

3.1. Site-scale analysis

We derived the optimal ε^*_{GPP} from linear regressions with no intercept between tower-measured GPP and modeled $f(\varepsilon) \times \text{PAR} \times \text{FPAR}$ products (Figure 2). Using the model setup of Local-EVI500, the derived ε^*_{GPP} values for corn and soybean are 3.18 gC MJ^{-1} and 1.91 gC MJ^{-1}, respectively. These values are approximately 3.1 and 1.8 times greater than the prescribed ε^*_{GPP} values of 1.04 gC MJ^{-1} in the MOD17A2 products. With recalibrated parameters, the MOD17 model is able to explain 67.9% of the GPP variances for corn and 77.4% for soybean. The results for each individual site are similar, and the model explains 62.3–80.8% of the GPP variance for corn and 51.2–88.4% for soybean (Table 3). The estimated ε^*_{GPP} values show site-to-site variability, and have a wider range for corn (2.44–3.94 gC MJ^{-1}) than for soybean (1.74–2.30 gC MJ^{-1}). For all studied sites, the derived ε^*_{GPP} estimates were higher than the value prescribed in MOD17A2.

Figure 3 compares the modeled GPP time series with the tower measurements. The peak GPP values from the tower measurements are 22.8 ± 2.2 gC m^{-2}d^{-1} for corn (yellow line), which was approximately 1.71 times greater than that of 13.3 ± 2.2 gC m^{-2}d^{-1} for soybean (green line). Note that the growing season starts earlier in MOD17A2

than flux tower GPP. A key reason is that MOD17A2 uses NCEP-DOE datasets while our modeling effort uses tower-measured meteorology data. This suggests that the MODIS GPP model is sensitive to the meteorological inputs as found in other studies (Sjöström et al., 2013; Zhao et al., 2005). Figure 3 also shows that the GPP time series from MOD17A2 (red line) does not capture the magnitude differences between corn and soybean fields. One reason is that the current version of the MOD17A2 product does not differentiate crop species under different photosynthetic pathways (C3 and C4). Using in situ meteorological measurements and recalibrated parameters, GPP estimates from the MOD17 model (blue line) agree with tower measurements for both corn and soybean. Results in Figures 2 and 3 indicate that applying crop-specific ε^*_g values is essential to obtain reasonable GPP estimates.

We used a Tylor diagram in Figure 4 to compare the performances for six model setups and MOD17A2 (Taylor, 2001). GPP estimates are compared regarding the phase (measured by correlation coefficients between the modeled and measured GPP), amplitude (measured by standard deviation), and accuracy (measured by root mean squared errors). The model setup of Local-EVI500 performs the best with the largest correlation coefficients (0.82 for corn and 0.88 for soybean). In line with other studies (Sjöström et al., 2013; Zhao and Running, 2010), our results find that the MOD17 model is sensitive to meteorological inputs. Modeling using tower meteorological measurements has higher correlation coefficients than using the NCEP-DOE Reanalysis II datasets. It is also evident that GPP estimates in MOD17A2 have much smaller standard deviations than other modeled results. Other factors have less influence on GPP estimation. Models at 1000 m result in slightly lower correlation coefficients than those at 500 m resolution, reflecting the effects of spatial variability due to the mismatches between the footprints of tower sites and MODIS pixels. Model setups using theMOD15-based and EVI-based FPAR achieve similar performance. Our findings indicate that the MOD17 model can be used to capture seasonal GPP variations; however, careful parameterization especially for ε^*_{GPP} is required.

3.2. Regional-scale analysis

In the regional-scale analysis, we derived cropland ε^*_{GPP} value based on regressions between GPP estimated from national inventory data and the modeled $\sum \text{PAR} \times \text{EVI} \times f(\varepsilon)$ products (Figure 5). We use total grain production instead of production per unit area in our regressions because large-scale studies usually focus on modeling total cropland GPP or yields. The derived cropland ε^*_{GPP} value is 2.06 gC MJ^{-1} when applying a general cropland mask and 2.23 gC MJ^{-1} when applying a fractional cropland map. Table 4 provides a full statistical summary of the four model setups in our regional study. The differences in the GPP estimates between EVI-based and MOD15-based FPAR are minor. The derived ε^*_{GPP} values are higher for corn than for soybean, which reflect the GPP differences between corn and soybean. The co-
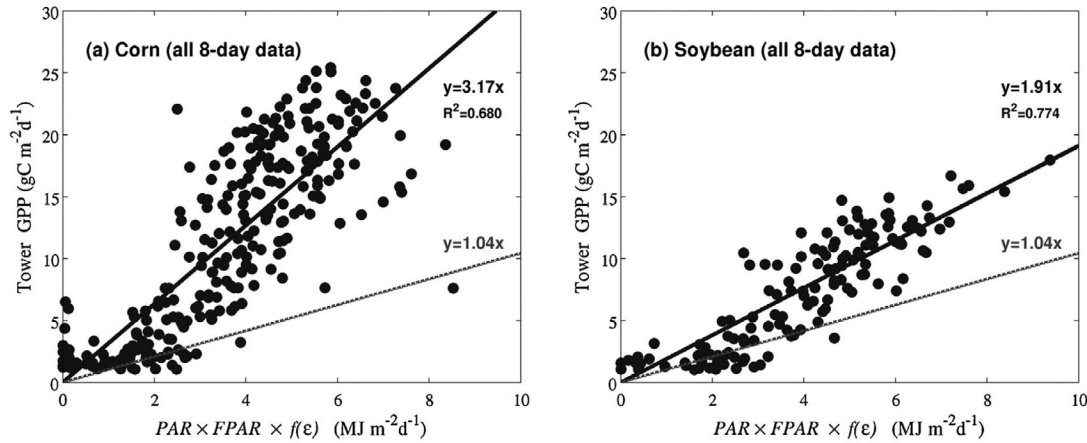
Figure 2. The 8-day GPP estimates from the flux tower measurements against modeled $f(\varepsilon) \times PAR \times FPAR$ for (a) corn and (b) soybean. This analysis includes all 8-day site-yearsdata during the vegetative season (GPP > 1 gC m^{-2}d^{-1}) and employs the model setup of Local-EVI500 (Table 2). Solid lines denote linear regressions without interception. Dashed lines denote lines with ε^*_{GPP} values used by MOD17A2.

Table 3. Statistical summary of the model performance for each individual site. The model setup of Local-EVI500 (Table 2 is used to derive the ε^*_{GPP} values using linear regressions without intercept. The coefficient of determination (R2), root mean squared error (RMSE), and mean error (ME) are reported for the 8-day GPP estimates.

	Corn				Soybean			
Site code	ε^*_{GPP} (gC MJ^{-1})	R^2	RMSE (gC m^{-2} d^{-1})	ME (gC m^{-2} d^{-1})	ε^*_{GPP} (gC MJ^{-1})	R^2	RMSE (gC m^{-2} d^{-1})	ME (gC m^{-2} d^{-1})
US-Bo1	2.44	0.711	3.452	−0.610	1.84	0.884	1.798	0.217
US-IB1	3.03	0.748	3.332	0.656	1.77	0.672	2.133	0.170
US-Ne1	3.47	0.701	3.893	0.422				
US-Ne2	3.41	0.778	3.339	0.533	2.02	0.788	2.199	0.397
US-Ne3	3.94	0.623	4.172	0.419	2.30	0.694	2.293	0.195
US-Ro1	3.01	0.702	3.860	0.758	1.74	0.512	1.957	0.116
US-Ro3	2.76	0.808	3.211	0.795				

efficients of determination (R^2) are greater when the fractional land use map is applied rather than a general mask. Similar to the site-scale studies, the derived ε^*_{GPP} values are higher than values prescribed in MOD17A2 for all model setups.

The spatial distributions of GPP estimates over the Midwestern US are shown in Figure 6. The annual GPP estimates from the MOD17A3 products are much lower than GPP modeled with recalibrated ε^*_{GPP} values. The spatial distribution of cropland GPP estimated by applying a general cropland ε^*_{GPP} value (Figure 6b) mainly reflects the climatic

gradients of the crop GPP. In this case, areas with more annual precipitation have higher cropland productivity. In comparison, modeled GPP estimates that apply crop-specific ε^*_{GPP} values and fractional land use maps (Figure 6c) are able to capture the variations of crop type and area at the sub-pixel level. For example, pixels with more corn covers in central Illinois have higher annual GPP estimates.

Figure 7 further compares modeled GPP with national inventory data. Annual GPP estimates derived from national inventory data in 2011 are 1848.4 ± 298.1 gC m^{-2}y^{-1} for corn and 908.9 ± 166.3 gC

Table 4. Statistical summary for the model performance from 2009 to 2012. ε^*_{GPP} values are derived based on the slope of linear regressions. The model setups are specified in Table 2.

| Model	Year	Cropland			Corn			Soybean		
		ε^*_{GPP} (gC/MJ)	R^2	RMSE (10^{12} gC/y)	ε^*_{GPP} (gC/MJ)	R^2	RMSE (10^{12} gC/y)	ε^*_{GPP} (gC/MJ)	R^2	RMSE (10^{12} gC/y)
MOD15-Mask	2009	1.95	0.884	0.235	3.38	0.781	0.262	1.83	0.496	0.122
	2010	1.67	0.877	0.234	2.76	0.779	0.245	1.64	0.589	0.117
	2011	1.74	0.835	0.274	2.81	0.841	0.217	1.72	0.387	0.130
	2012	1.84	0.660	0.373	3.06	0.709	0.273	2.02	0.567	0.112
MOD15-Frac	2009	2.09	0.867	0.252	2.83	0.929	0.149	1.22	0.877	0.060
	2010	1.79	0.865	0.245	2.32	0.898	0.167	1.13	0.897	0.058
	2011	1.86	0.811	0.293	2.43	0.897	0.175	1.12	0.778	0.078
	2012	1.95	0.622	0.393	2.47	0.639	0.304	1.31	0.788	0.079
EVI-Mask	2009	2.20	0.884	0.236	3.78	0.761	0.274	2.09	0.562	0.114
	2010	2.00	0.874	0.237	3.29	0.772	0.249	1.97	0.618	0.112
	2011	2.06	0.847	0.264	3.29	0.818	0.232	2.08	0.475	0.120
	2012	2.28	0.680	0.362	3.77	0.720	0.268	2.49	0.592	0.109
EVI-Frac	2009	2.38	0.878	0.242	3.20	0.926	0.152	1.39	0.903	0.053
	2010	2.15	0.868	0.242	2.79	0.894	0.169	1.36	0.908	0.055
	2011	2.23	0.834	0.275	2.89	0.898	0.174	1.36	0.831	0.068
	2012	2.43	0.647	0.380	3.07	0.658	0.296	1.64	0.810	0.074
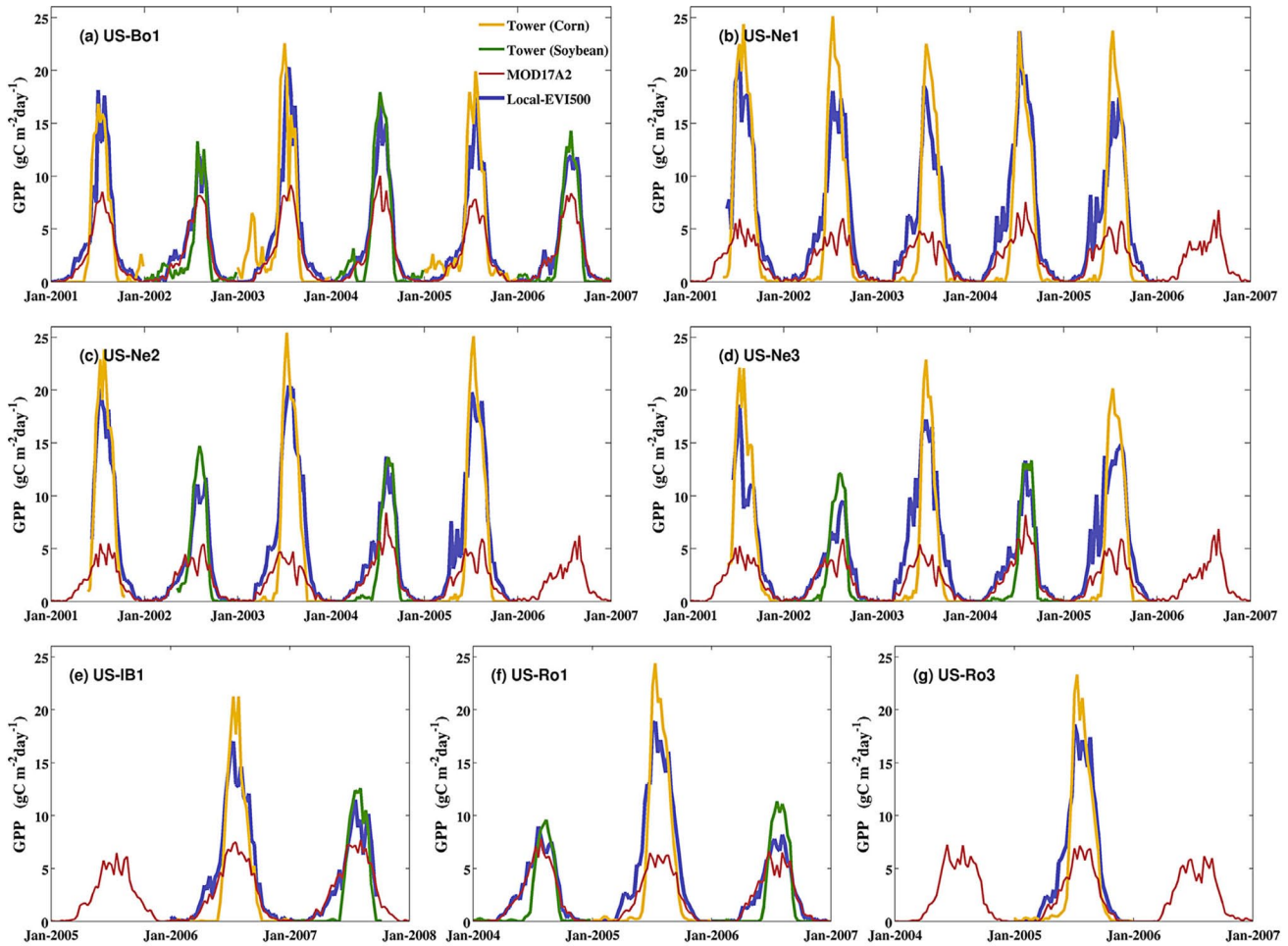
Figure 3. Time series of GPP estimates at the seven tower sites. The yellow and green lines denote the tower-based GPP estimates for corn and soybean, respectively. The blue lines denote the modeled GPP estimates based on the Local-EVI500 model setup. The red lines denote the GPP estimates from the Collection 5.1 MOD17A2 products.

m^{-2}y^{-1} for soybean, which are approximately 2.28 and 1.15 times greater than GPP estimates in the MOD17A3 products (810.7 ± 98.7 gC m^{-2}y^{-1} for corn and 790.3 ± 113.8 gC m^{-2}y^{-1} for soybean). Methods that apply a general cropland mask tend to overestimate GPP for both corn and soybean. By comparison, modeled GPP estimates based

on fractional land-use maps generally match national inventory references. The modeled annual GPP (MOD15-Frac) are 1887.8 ± 229.8 gC m^{-2}y^{-1} for corn and 849.1 ± 122.2 gC m^{-2}y^{-1} for soybean. These results indicate that integrating fine-resolution land use maps could improve regional GPP modeling.
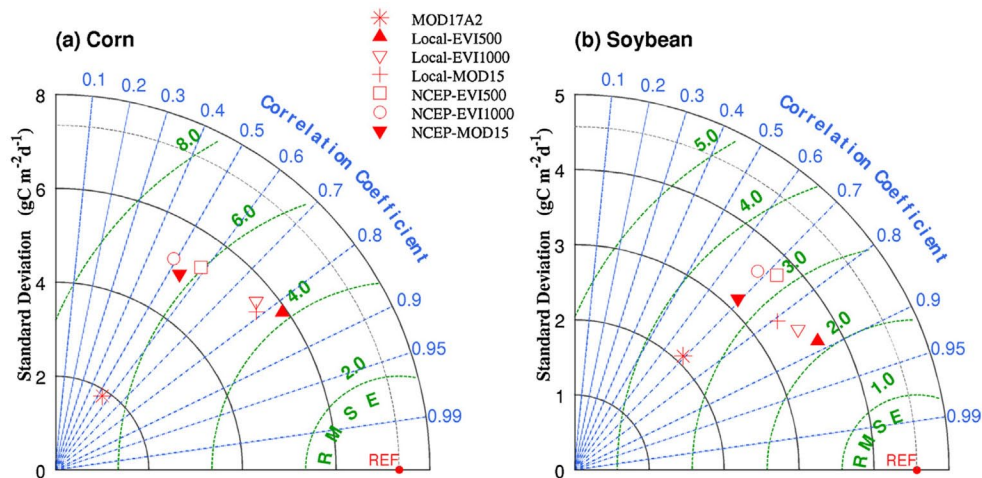

Figure 4. Statistical comparison of the model performances in a Taylor diagram. Results from six model setups based on the MOD17 model (Table 2) are compared with MOD17A2. The correlation coefficient (r), standard deviation (gC m^{-2}d^{-1}) and root mean squared errors (gC m^{-2}d^{-1}) are calculated using all site-years data. The "REF" symbol indicates GPP references from the tower measurements.
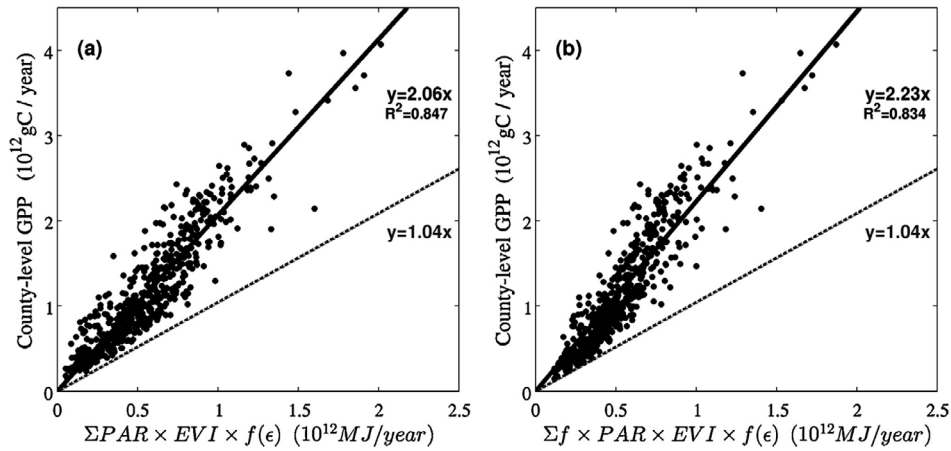
Figure 5. Annual GPP derived from the 2011 national inventory data are plotted against the modeled PAR × EVI × $f(\varepsilon)$ products by applying (a) a general cropland mask (EVI-Mask) and (b) a fractional cropland map (EVI-Frac). Solid lines denote linear regressions with no intercepts. Dashed lines denote lines with the ε^*_{GPP} values used by MOD17A2.
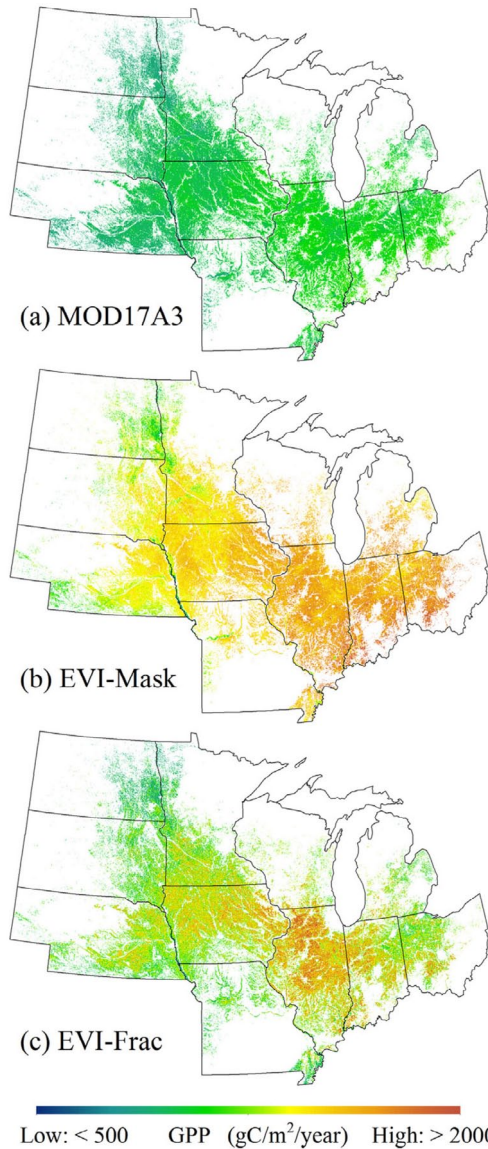

Figure 6. The spatial distribution of annual cropland GPP in 2011 as derived by (a) the yearly MODIS GPP products (MOD17A3), (b) the EVI-Mask model setup with a general cropland ε^*_{GPP}, and (c) the EVI-Frac model setup with crop-specific ε^*_{GPP}.
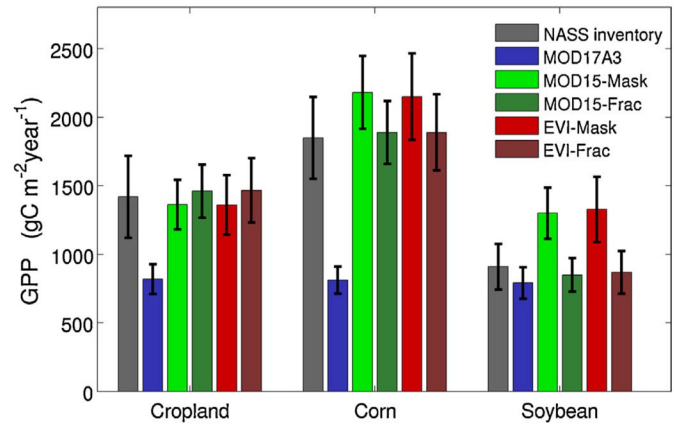

Figure 7. GPP estimates (mean ± standard deviation) in 2011 as derived from NASS inventory data and modeled by MOD17A3 and different model setups. The model setups are specified in Table 2. Standard deviations of MODIS GPP estimates are derived using all pixels that have subpixel proportions of corn or soybean greater than 50%.

4. Discussion

4.1. LUE in field measurements and in remote sensing models

Some large-scale studies have cautioned the use of field-derived LUE values in remote sensing models. For the United States, Lobell et al. (2002) calibrated LUE values in the CASA model using Advanced Very High Resolution Radiometer (AVHRR) satellite data with agricultural survey data. Their derived ε^*_{GPP} values after translation were only 1.43 ± 0.27 gC MJ^{-1} for corn and 0.63 ± 0.20 gC MJ^{-1} for non-corn areas. Bradford et al. (2005) also found that the LUE values estimated from the AVHRR data were well below the values that were derived from field measurements. In these studies, the large discrepancies between the LUE values in remote sensing models and field measurements were attributed to the biased location selection in field measurements and the overestimated APAR values in satellite-based studies. However, we observe that the ε^*_{GPP} values derived from inventory data are consistent with those derived from the flux tower data (Figure 8). In our best fit with the tower-based GPP reference, the ε^*_{GPP} values are 2.78 ± 0.48 gC MJ^{-1} for corn and 1.64 ± 0.23 gC MJ^{-1} for soybean based on the Local-MOD15 model. When using the inventory-based
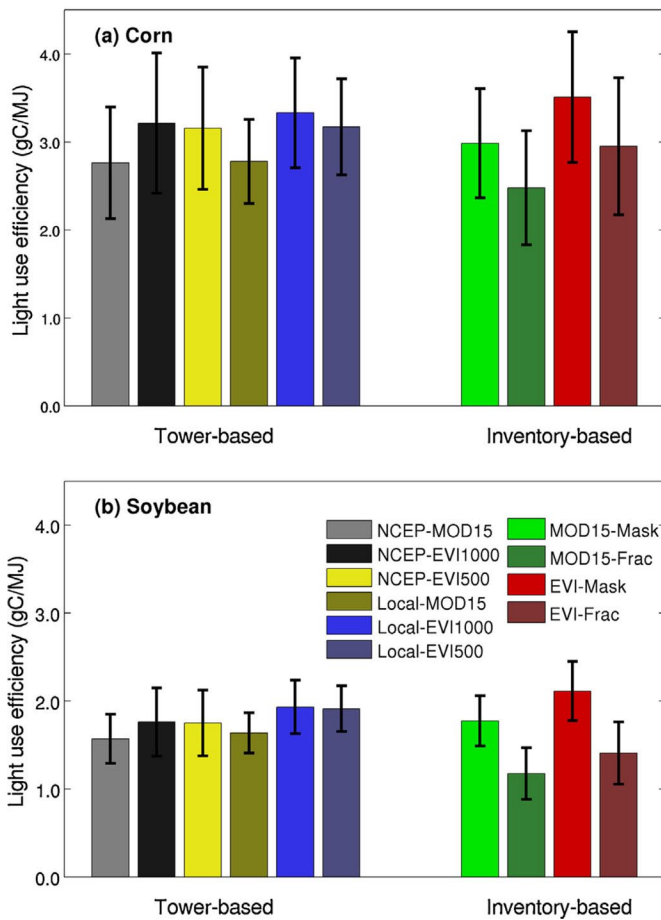
Figure 8. Comparisons of the derived ε^*_{GPP} values based on different model setups for (a) corn and (b) soybean. Standard deviations are calculated based on data from all site-years and county-years.

GPP references, the derived ε^*_{GPP} values are 2.48 ± 0.65 gC MJ^{-1} for corn and 1.18 ± 0.29 gC MJ^{-1} for soybean using the MOD15-Frac model. All these values fall within the range of field-measured results as reviewed by Sinclair and Muchow (1999).

Though different from early studies using AVHRR data (Bradford et al., 2005; Lobell et al., 2002), our findings show agreement with recent studies (Bandaru et al., 2013; Chen et al., 2011; Guanter et al., 2014) and indicate that the field-derived ε^*_{GPP} values should be consistently used for large-scale modeling. In our results (Figures 2 and 5), it is clear that the underestimated MODIS GPP is largely due to the underestimated ε^*_{GPP}. The MODIS Land Science team has made tremendous efforts on model parameterization in a generalized manner to characterize global biomes, such that the ε^*_{GPP} values prescribed in the current MODIS GPP products do not vary with geographical location. Our evaluation efforts imply that there is a need to readjust the parameters in the MOD17 model carefully for studies in specific regions, especially agricultural zones.

4.2. Uncertainties of ε^*_{GPP} estimates in regional modeling

Several factors may influence the inversion of the MOD17 model for deriving optimal cropland ε^*_{GPP} values in our study. First, we did not try to alter the MOD17 model structure, which uses *TMIN* and *VPD* to ac-

count for climatic stresses. Other PEMs used slightly different climate variables to down-regulate LUE estimates (Cramer et al., 1999; Wu et al., 2010), and recent studies also tried to estimate LUE directly from remote sensing data (Hilker et al., 2008, 2010). To understand the influences of environmental factors on the modeled results, we also perform model calibrations without environmental LUE limitations (i.e., without $f(\varepsilon)$ in Eq. (1)) using the Local-MOD15 model setup. The derived LUE values are 2.31 gC MJ^{-1} for corn and 1.37 gC MJ^{-1} for soybean, which are approximately 16.9% and 16.5% lower than the models with environmental LUE down-regulations, respectively.

Second, the general cropland mask defined by a threshold of 50% influences regional GPP modeling. When the cropland mask is defined based on thresholds of 40% or 60%, the calibrated cropland ε^*_{GPP} values using the MOD15-Mask model setup are 2.06 ± 0.15 gC MJ^{-1} or 1.60 ± 0.10 gC MJ^{-1}, which are approximately 14.4% higher or 11.2% lower, respectively, than when a threshold of 50% is applied (Table 4). The method that applies fractional land use maps circumvents the threshold problem and provides reliable ε^*_{GPP} and GPP estimates (Figures 7 and 8). Even the NASS CDL data routinely produce fine-resolution land use maps on an annual basis, successful algorithms that can produce global crop-specific maps at fine resolutions remain to be developed (Yu et al., 2013; Zhong et al., 2011).

Finally, satellite-derived FPAR also influence the ε^*_{GPP} estimates. Models with EVI-based FPAR perform better than the MOD15-based FPAR in terms of the explained GPP variance (Figure 4). However, ε^*_{GPP} values derived from EVI-based FPAR are approximately 14–25% greater than values derived from the MOD15-based FPAR (Tables 3 and 4). Similar to previous studies (Kalfas et al., 2011; Xiao et al., 2004), the constant in Eq. (6) for estimating the FPAR was assumed to be 1.0. Additional field studies are necessary for quantifying the relationships between EVI and FPAR for different crop species.

5. Conclusions

Satellite remote sensing provides an efficient method for monitoring vegetation GPP at a large scale. However, parameterization of the light use efficiency varies considerably for croplands. Based on the MOD17 model, we evaluate ε^*_{GPP} values at multi scales using both in situ measurements and inventory data.

We observed consistent LUE values from both site and regional-scale models. The derived ε^*_{GPP} values based on the 28 site-years tower measurements are 2.78 ± 0.48 gC MJ^{-1} for corn and 1.64 ± 0.23 gC MJ^{-1} for soybean. Calibrations using 4-year inventory data generate ε^*_{GPP} values of 2.48 ± 0.65 gC MJ^{-1} for corn and 1.18 ± 0.29 gC MJ^{-1} for soybean. The environmental factors account for approximately 16% uncertainties of the ε^*_{GPP} estimates. The general cropland mask with varying thresholds (0.40–0.60) accounts for 11–14% of the uncertainty in the GPP estimates. The different methods that are used to derive FPAR from satellite data may generate 14–25% uncertainties of ε^*_{GPP}. Given the results from both tower measurements and inventory data, we conclude that field-derived LUE values should be used consistently in large-scale modeling.

We also observed that the MODIS GPP products are underestimated for croplands in the Midwestern US. Using model setups similar to the MOD17 GPP product, the derived ε^*_{GPP} value is 1.80 ± 0.12 gC MJ^{-1}, or 1.73 times greater than the value prescribed in the current MOD17 GPP model. With recalibrated ε^*_{GPP} values, the modeled annual GPP could match national inventory data. These results suggest that the parameters (primarily ε^*_{GPP}) in the MOD17 model should be carefully readjusted to characterize cropland GPP in the Midwestern US.

References

Bandaru, V., West, T.O., Ricciuto, D.M., César Izaurralde, R., 2013. Estimating crop net primary production using national inventory data and MODIS-derived parameters. ISPRS J. Photogramm. Remote Sens. 80, 61–71.

Beer, C., et al., 2010. Terrestrial gross carbon dioxide uptake: Global distribution and covariation with climate. Science 329 (5993), 834–838.

Boryan, C., Yang, Z., Mueller, R., Craig, M., 2011. Monitoring US agriculture: The US Department of Agriculture, National Agricultural Statistics Service, cropland data layer program. Geocarto Int. 26 (5), 341–358.

Bradford, J., Hicke, J., Lauenroth, W., 2005. The relative importance of light-use efficiency modifications from environmental conditions and cultivation for estimation of large-scale net primary productivity. Remote Sens. Environ. 96 (2), 246–255.

Chen, T., van der Werf, G.R., Dolman, A.J., Groenendijk, M., 2011. Evaluation of crop-land maximum light use efficiency using eddy flux measurements in North America and Europe. Geophys. Res. Lett., 38.

Choudhury, B.J., 2000. Carbon use efficiency, and net primary productivity of terrestrial vegetation. Adv. Space Res. 26 (7), 1105–1108.

Cramer, W., et al., 1999. Comparing global models of terrestrial net primary productivity (NPP): Overview and key results. Global Change Biol. 5 (S1), 1–15.

Field, C.B., Randerson, J.T., Malmstrom, C.M., 1995. Global net primary production: Combining ecology and remote sensing. Remote Sens. Environ. 51 (1), 74–88.

Garbulsky, M.F., et al., 2010. Patterns and controls of the variability of radiation use efficiency and primary productivity across terrestrial ecosystems. Global Ecol. Biogeogr. 19 (2), 253–267.

Gelybó, G., Barcza, Z., Kern, A., Kljun, N., 2013. Effect of spatial heterogeneity on the validation of remote sensing based GPP estimations. Agric. For. Meteorol. 174, 43–53.

Goetz, S.J., Prince, S.D., Goward, S.N., Thawley, M.M., Small, J., 1999. Satellite remote sensing of primary production: An improved production efficiency modeling approach. Ecol. Model. 122 (3), 239–255.

Gower, S., et al., 2001. Net primary production and carbon allocation patterns of boreal forest ecosystems. Ecol. Appl. 11 (5), 1395–1411.

Griffis, T., Baker, J., Sargent, S., Tanner, B., Zhang, J., 2004. Measuring field-scale isotopic CO_2 fluxes with tunable diode laser absorption spectroscopy and micrometeorological techniques. Agric. For. Meteorol. 124 (1), 15–29.

Guanter, L., et al., 2014. Global and time-resolved monitoring of crop photosynthesis with chlorophyll fluorescence. Proc. Natl. Acad. Sci. U. S. A. 111 (14), E1327–E1333.

Heinsch, F.A., et al., 2003. User's Guide: GPP and NPP (MOD17A2/A3) Products, NASAMODIS Land Algorithm, Version 2.0, pp. 1–57.

Hilker, T., Coops, N.C., Wulder, M.A., Black, T.A., Guy, R.D., 2008. The use of remote sensing in light use efficiency based models of gross primary production: A review of current status and future requirements. Sci. Total Environ. 404 (2), 411–423.

Hilker, T., et al., 2010. Remote sensing of photosynthetic light-use efficiency across two forested biomes: Spatial scaling. Remote Sens. Environ. 114 (12), 2863–2874.

Huete, A., et al., 2002. Overview of the radiometric and biophysical performance of the MODIS vegetation indices. Remote Sens. Environ. 83 (1–2), 195–213.

Kalfas, J.L., Xiao, X., Vanegas, D.X., Verma, S.B., Suyker, A.E., 2011. Modeling gross primary production of irrigated and rain-fed maize using MODIS imagery and CO_2 flux tower data. Agric. For. Meteorol. 151 (12), 1514–1528.

Lindquist, J.L., Arkebauer, T.J., Walters, D.T., Cassman, K.G., Dobermann, A., 2005. Maize radiation use efficiency under optimal growth conditions. Agron. J. 97(1), 72–78.

Lobell, D.B., et al., 2002. Satellite estimates of productivity and light use efficiency in United States Agriculture, 1982–98. Global Change Biol. 8 (8), 722–735.

Matamala, R., Jastrow, J.D., Miller, R.M., Garten, C., 2008. Temporal changes in C and N stocks of restored prairie: Implications for C sequestration strategies. Ecol. Appl. 18 (6), 1470–1488.

Meyers, T.P., Hollinger, S.E., 2004. An assessment of storage terms in the surface energy balance of maize and soybean. Agric. For. Meteorol. 125 (1), 105–115.

Myneni, R.B., et al., 2002. Global products of vegetation leaf area and fraction absorbed PAR from year one of MODIS data. Remote Sens. Environ. 83 (1–2), 214–231.

Potter, C.S., et al., 1993. Terrestrial ecosystem production – A process model-based on global satellite and surface data. Global Biogeochem. Cycles 7 (4), 811–841.

Prince, S.D., Goward, S.N., 1995. Global primary production: A remote sensing approach. J. Biogeogr. 22 (4–5), 815–835.

Prince, S.D., Haskett, J., Steininger, M., Strand, H., Wright, R., 2001. Net primary production of US Midwest croplands from agricultural harvest yield data. Ecol. Appl.11 (4), 1194–1205.

Reeves, M.C., Zhao, M., Running, S.W., 2005. Usefulness and limits of MODIS GPP for estimating wheat yield. Int. J. Remote Sens. 26 (7), 1403–1421.

Reichstein, M., et al., 2005. On the separation of net ecosystem exchange into assimilation and ecosystem respiration: Review and improved algorithm. Global Change Biol. 11 (9), 1424–1439.

Ruimy, A., Saugier, B., Dedieu, G., 1994. Methodology for the estimation of terrestrial net primary production from remotely sensed data. J. Geophys. Res. Atmos. 99(D3), 5263–5283.

Running, S.W., et al., 2004. A continuous satellite-derived measure of global terrestrial primary production. Bioscience 54 (6), 547–560.

Running, S.W., Thornton, P.E., Nemani, R., Glassy, J.M., 2000. Global terrestrial gross and net primary productivity from the earth observing system. Methods Ecosyst. Sci., 44–57.

Schlesinger, W.H., Bernhardt, E.S., 2013. Biogeochemistry: An Analysis of Global Change. Elsevier.

Sinclair, T.R., Muchow, R.C., 1999. Radiation use efficiency. Advances in Agronomy 65, 215–265.

Singer, J.W., Meek, D.W., Sauer, T.J., Prueger, J.H., Hatfield, J.L., 2011. Variability of light interception and radiation use efficiency in maize and soybean. Field Crops Res. 121 (1), 147–152.

Sjöström, M., et al., 2013. Evaluation of MODIS gross primary productivity for Africa using eddy covariance data. Remote Sens. Environ. 131, 275–286.

Suyker, A.E., Verma, S.B., 2012. Gross primary production and ecosystem respiration of irrigated and rainfed maize–soybean cropping systems over 8 years. Agric. For. Meteorol. 165, 12–24.

Taylor, K.E., 2001. Summarizing multiple aspects of model performance in a single diagram. J. Geophys. Res. Atmos. (1984–2012) 106 (D7), 7183–7192.

Turner, D.P., Gower, S.T., Cohen, W.B., Gregory, M., Maiersperger, T.K., 2002. Effects of spatial variability in light use efficiency on satellite-based NPP monitoring. Remote Sens. Environ. 80 (3), 397–405.

Turner, D.P., et al., 2006. Evaluation of MODIS NPP and GPP products across multiple biomes. Remote Sens. Environ. 102 (3), 282–292.

Wu, C., Munger, J.W., Niu, Z., Kuang, D., 2010. Comparison of multiple models for estimating gross primary production using MODIS and eddy covariance data in Harvard Forest. Remote Sens. Environ. 114 (12), 2925–2939.

Xiao, X.M., et al., 2004. Satellite-based modeling of gross primary production in an evergreen needleleaf forest. Remote Sens. Environ. 89 (4), 519–534.

Xin, Q., et al., 2013. A production efficiency model-based method for satellite estimates of corn and soybean yields in the midwestern US. Remote Sens. 5 (11),5926–5943.

Yang, Y., Shang, S., Guan, H., Jiang, L., 2013. A novel algorithm to assess gross primary production for terrestrial ecosystems from MODIS imagery. J. Geophys. Res.: Biogeosci. 118 (2), 590–605.

Yu, L., et al., 2013. FROM-GC: 30 m global cropland extent derived through multi-source data integration. Int. J. Digit. Earth 6, 521–533.

Zhang, Q., et al., 2014. Estimation of crop gross primary production (GPP): I. Impact of MODIS observation footprint and impact of vegetation BRDF characteristics. Agric. For. Meteorol. 191, 51–63.

Zhang, Y., Yu, Q., Jiang, J., Tang, Y., 2008. Calibration of Terra/MODIS gross primary production over an irrigated cropland on the North China Plain and an alpine meadow on the Tibetan Plateau. Global Change Biol. 14 (4), 757–767.

Zhao, M., Heinsch, F.A., Nemani, R.R., Running, S.W., 2005. Improvements of the MODIS terrestrial gross and net primary production global data set. Remote Sens. Environ. 95 (2), 164–176.

Zhao, M., Running, S.W., 2010. Drought-induced reduction in global terrestrial net primary production from 2000 through 2009. Science 329 (5994), 940–943.

Zhong, L., Hawkins, T., Biging, G., Gong, P., 2011. A phenology-based approach to map crop types in the San Joaquin Valley, California. Int. J. Remote Sens. 32 (22), 7777–7804.